# 2 Effect of Womersley number on transition to

# 3 turbulence in pipe flow: an experimental study.

# Baha Al-Deen T. El-Khader<sup>1</sup>, Melissa C. Brindise<sup>1\*</sup>

<sup>1</sup> The Pennsylvania State University, Department of Mechanical Engineering, University Park, PA, USA

#### \*mcb5351@psu.edu

# Abstract

The mechanisms driving transition to turbulence in pulsatile flows are not well understood. Prior studies in this domain have noted the dynamics of this flow regime to depend on the mean Reynolds number, pulsation frequency (i.e., Womersley number), and inflow pulsatile waveform shape. Conflicting findings particularly regarding the role of Womersley number on critical Reynolds number and the development of turbulence have been reported. The discord has primarily been observed for flows with Womersley numbers ranging from 4 to 12. Hence, in this work, we use particle image velocimetry to explore the effects of Womersley number within this 4 to 12 range on the dynamics of pulsatile transition. Eighteen total test cases were captured using six mean Reynolds numbers (range 800-4200) and five Womersley numbers. Turbulent kinetic energy (TKE), turbulence intensity (TI), and phase lag were computed. Our results indicated critical Reynolds number was roughly independent of Womersley number. At high Womersley numbers, the TI trend maintained lower pulsatility and the flow was observed to mimic a steady transitional flow regime. A plateau of the TI-velocity and TI-acceleration phase lag was observed at a Womersley number of 8, highlighting that this may be the critical value where further increases to Womersley number do not alter the transition dynamics. Further, this suggests

- that phase lag may provide a universal indicator on the specific influence of Womersley number on
- 2 transition for a given flow. Overall, these findings elucidate critical details regarding the role of
- 3 Womersley number on transition to turbulence.

# 1 Introduction

Transitional and fluctuating flow behaviors in pulsatile (non-steady) flows have been observed to occur across a variety of applications such as biomedical, environmental, thermodynamic devices, and internal combustion flows. Transitional flows have been demonstrated to cause significant fluctuations in flow parameters such as wall shear stress (WSS) and pressure. For biomedical flows, this affects the life cycle of aneurysms and the development of stenosis 4-6. Also, transition-induced instabilities can affect the efficiency of heat exchange systems in research reactors and performance of fuel cells. Moreover, transitional flows can precipitate adversarial effects such as weakening materials to failure and causing performance reduction. Hence, in these applications, it is often important to quantify or estimate the role and influence of transition-induced flow fluctuations to mitigate their highlighted adversarial effects. However, the fundamental mechanisms driving transition to turbulence in pulsatile flows remain largely unknown.

Pulsatile flow is defined as a constant mean flow component with a superimposed oscillating flow component. Many studies have investigated pulsating turbulent flows such that the effects of pulsation frequency on the development and dynamics of turbulent structures in turbulent flows has been well documented. Specifically, at high Womersley numbers (Wo≥10), multiple studies have observed 'frozen' turbulent structures (as described by He and Jackson (2009)¹0), i.e. the turbulent structures resemble those observed in turbulent steady flow. This is due to insufficient time for structures to relaminarize during the acceleration phase at such high Womersley numbers.¹¹0-1² At high Womersley numbers, turbulence and fluctuations are produced and confined near the wall region. ¹¹0-1³ Scotti and Piomelli (2001) proposed a parameter—turbulent stokes length—to measure the length of that near wall

region. This parameter is proportional to the molecular and turbulent diffusivities and inversely proportional to the frequency of pulsation. Hence, as Womersley number is decreased, these fluctuations increasingly propagate from the wall to the core region. 10,11,14 Womersley number has also been noted to affect the shape of turbulent structures as well as the fluctuating velocity contours at different phases of the cycle. At high Womersley numbers, very long and low speed streak-shaped fluctuating velocity contours are present during the acceleration phase. During the deceleration phase, these streaks persisted, although shorter. However, at low Womersley numbers, studies observed a very small number of fluctuations at the start of acceleration phase, but by the second half of the acceleration phase long streaks (similar to those observed at high Womersley number) had formed. However, these structures destabilize with time and burst, spreading turbulence across the flow by the end of acceleration. Thus, these studies highlight that Womersley number affects the fundamental turbulent mechanics in pulsatile flows.

As opposed to the fully turbulent regime, only a small number of studies have investigated transitional pulsatile flows. Among the studies that have been done, they have emphasized that the onset and development of transition in pulsatile flows is affected by mean Reynolds number (Re), <sup>15</sup> Womersley number, <sup>2,12,16-18</sup> pulsatile waveform shape, <sup>19,20</sup> and the initial conditions. <sup>16</sup> However, consensus regarding the specific role of each parameter has not been reached. In particular, studies evaluating the effect of Womersley number have produced significantly conflicting findings. In agreement with fully turbulent flow findings, several studies noted that transitional flow behavior mimicked steady flow at high Womersley numbers. For example, Xu and Avila (2018) reported the lifetime and propagation speed of turbulent puffs were similar to that of steady flow for high Womersley numbers (Wo=17.7)<sup>16</sup>. At low Womersley numbers, turbulent puffs shrink during the acceleration phase of the cycle and grow during the deceleration phase, suggesting a phase lag between turbulence intensity (TI) and velocity exists. <sup>16</sup> Previous studies investigated the TI-velocity phase lag and reported inconsistent values of phase lag at different Womersley numbers. Trip et al (2012) reported a 180° phase lag (relative to bulk velocity) at

Wo=15 and at Wo=20;<sup>15</sup> they reported phase lag to be independent of mean Reynolds number, oscillatory Reynolds number, and Womersley number. On the other hand, Iguchi et al (1993) investigated pulsatile pipe flow at Wo=4.85 and reported 0° phase lag near the wall region and moving away from the wall they reported an increase in phase lag reaching a peak at the core region. Although Iguchi et al (1993) didn't test other Womersley numbers, they speculated that pulsation frequency will affect phase lag as at higher frequencies there will be a smaller time window for turbulence to propagate from the wall to the core region.<sup>14</sup> Some minor discrepancies regarding the shape of turbulent puffs have been reported.<sup>15</sup> <sup>18</sup> Specifically, Stettler and Hussain (1986) reported phase locked inverted puffs at low Womersley numbers.<sup>18</sup> However, Trip et.al (2012) and Xu et.al observed phase locked upright puffs at similar Womersley numbers. 15,17 Considerable inconsistencies regarding the relationship between Womersley number and the critical Reynolds number have been reported. Peacock et al. (1998) reported that critical Reynolds number monotonically increased with increasing Womersley number in the range of 4-20.<sup>2,21</sup> Stettler and Hussain (1986) as well as Sarpkaya (1966) reported that the peak critical Reynolds number occurred at a Womersley number of 4-5 and critical Reynolds number decreased for Womersley numbers in the range of 6–10 and increased for Womersley numbers in the range of 1–4. 18,22 Xu et al. (2017) reported critical Reynolds number monotonically decreased in the Womersley number range of 3–10; outside of this range, the two variables were independent. Trip et al. (2012) and Stettler and Hussain (1986) also observed that critical Reynolds number was independent of Womersley number for Womersley numbers in the range of 10-25.15 Xu and Avila (2018) reported critical Reynolds number to be nearly independent of Womersley number, except in the Womersley number range of 4-6 (full tested range of 2–18). These wide discrepancies highlight that the underlying physics of pulsatile transitional flows remain an ongoing and open investigation. Moreover, much of the discord is observed to center around Womersley numbers in the range of 4–10. In this work, we investigate the fundamental flow differences observed in pulsatile transitional flows within this discrepant Womersley number range, with the goal of identifying key Womersley number effects and changepoints. Specifically, we tested cases across five different Womersley numbers (range

1

2

3

4

5

6

7

8

9

10

11

12

13

14

15

16

17

18

19

20

21

22

23

24

25

- of 4–12) and six mean Reynolds numbers (range of 800–4200). Planar particle image velocimetry (PIV)
- 2 was used for this study. For each test case, we compared the flow structure by analyzing velocity profiles
- 3 and coherent structures. Transitional and turbulent flow development was characterized using turbulent
- 4 kinetic energy (TKE) and TI. Additionally, we investigated the phase lag between TI-inflow waveform
- 5 velocity and TI-inflow waveform acceleration.

#### 2 Methods

6

7

8

9

10

11

12

13

14

Figure 1 shows a schematic of the flow loop and PIV setup used for this study. The test section consisted of a straight and rigid tube (FEP - fluorinated ethylene propylene) with a 1/4" inner diameter and 1/8" wall thickness. To ensure the flow at the test section was fully developed, the flow loop contained a 190-diameter length of the tubing upstream of the test section. A sinusoidal inflow waveform was used for all test cases. A computer-controlled gear pump generated the desired flow. An ultrasonic flowmeter (Transonic) was placed upstream of the test section, while pressure transducers (Omega, PX309) were placed before and after the test section to monitor the flow loop properties. Water, with a

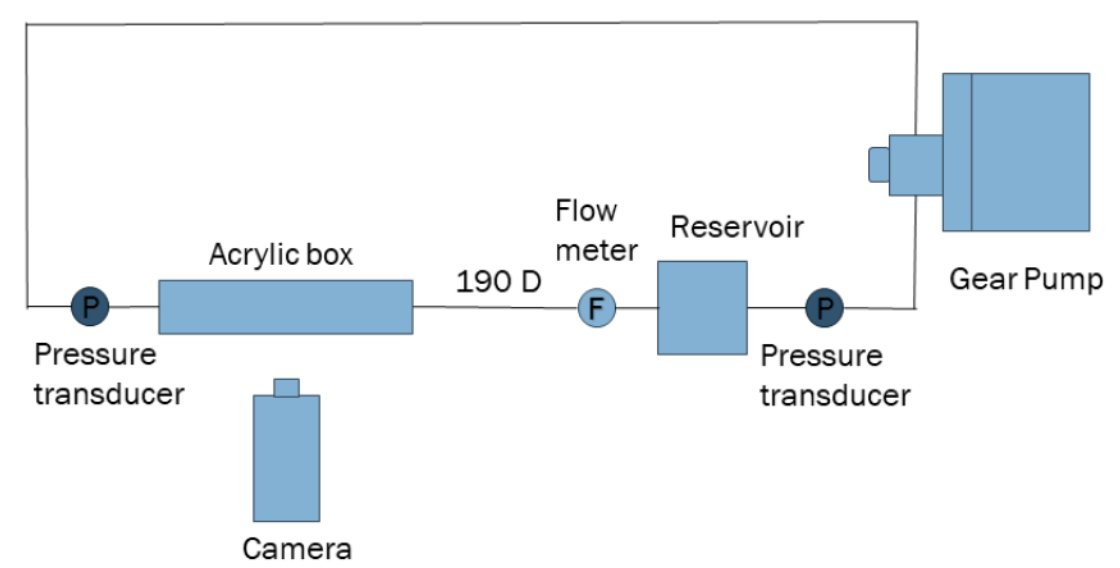


Figure 1. Flow loop and planar particle image velocimetry experimental schematic. The test section was submerged in a box filled with working fluid, and the laser sheet vertically pierced the center of the pipe. F and P denote the locations of the flowmeter probe and pressure transducers, respectively.

density of 997 kg/m<sup>3</sup> and kinematic viscosity of 1.108 × 10<sup>-6</sup> m<sup>2</sup>/s, was used as the working fluid. Water

and FEP maintain the same index of refraction; hence, by using water as the working fluid and submerging the test section in water, optical distortions in the PIV images were minimized.

A total of 18 test cases were measured; this included five Womersley numbers (Wo) (4, 6, 8, 10, and 12) and six mean Reynolds numbers, (800, 2300, 2500, 2700, 3200, and 4200), where Womersley number  $(\alpha)$  and mean Reynolds number (Rem) are defined by Eq. 1 and 2, respectively.

$$\alpha = R\sqrt{2\pi f/v} \tag{1}$$

$$Re_m = u_m D/v \tag{2}$$

where the velocity u is composed of a mean velocity component  $u_m$  and an oscillatory velocity

Table 1 Test matrix for all cases investigated in this experiment.

	Wo=4	Wo= 6	Wo= 8	Wo= 10	Wo= 12
$Re_m = 800$	✓	-	-	-	✓
$Re_m = 2300$	✓	✓	✓	✓	✓
$Re_m = 2500$	✓	-	-	-	✓
$Re_m = 2700$	✓	✓	✓	✓	✓
$Re_m = 3200$	✓	-	-	-	✓
$Re_m = 4200$	✓	-	-	-	✓

component  $u_o$ , D is the diameter of the pipe,  $\boldsymbol{v}$  the kinematic viscosity, and f is the frequency of pulsation for the input flow waveforms. The Womersley number and mean Reynolds number ranges were chosen based on previous literature and experimental setup limitations. For Womersley number, multiple previous studies<sup>15–18</sup> agreed that transition is independent of Womersley number and steady flow dynamics are recovered for Wo  $\geq 10$ . Additionally, much of the disagreement regarding the effect of Womersley number on transition has been reported within the selected range for this study (4-12). For

Reynolds number, the chosen values were inferred from the findings of Trip et al. (2012)<sup>15</sup>, who reported transition to occur within mean Reynolds numbers of 2300-2700 across many Womersley numbers. Therefore, we included a case at a considerably lower mean Reynolds number (800) and a considerably higher mean Reynolds number (4200) to span the laminar, transitional, and turbulent regimes. Moreover, four mean Reynolds numbers were selected within the expected transitional regime<sup>15</sup> to enable an indepth investigation of transitional flow dynamics and trends. Hence, these selected ranges, we were able to quantify and contrast the effect of Womersley number on pipe flow for different regimes. The test matrix is given in Table 1. For all test cases, the oscillating Reynolds number,  $Re_o = u_o D/v$ , was set to be 800 (i.e., a mean Reynolds number case of 800 would have an instantaneous Reynolds number range of 0-1600 through the pulsatile cycle). Figure 2 shows the inflow waveforms, as measured by the flowmeter, for the 800 mean Reynolds number, 4 and 12 Womersley number cases. PIV imaging was acquired using a high-speed camera (Phantom VEO440) and an Nd-YLF laser (Photonic Industries,  $\lambda = 527$  nm). Images of size 1024 x 1024 pixels were captured using a doublepulsed timing scheme. Image pairs were captured at a frequency of 750 Hz to ensure accurate temporal gradients could be calculated. The effective time interval between each image pair (dt) was set for each case to ensure a maximum particle displacement per frame of 8-12 pixels. Because Womersley number directly modulates the overall pulsatile cycle time, a different number of cycles for each Womersley number could be captured. This double-pulsed timing scheme ensured that at least 2 cycles were captured for the 4 Womersley number cases. For the 12 Womersley number cases, about 40 cycles were captured. The frame pair capture rate was not adjusted between test cases as this would alter the temporal resolution across test cases and could create a bias in the subsequent analysis. A laser sheet with a thickness of 1mm was precisely aligned with the center of the tube to minimize out-of-plane effects. The working fluid was seeded with 10 µm fluorescent particles, and the camera's magnification was set at 6.67 µm/pixel.

1

2

3

4

5

6

7

8

9

10

11

12

13

14

15

16

17

18

19

20

21

22

Prana, a publicly-available software (https://github.com/aether-lab/prana), was used to process the PIV images. Three passes of an image deformation algorithm were used<sup>23</sup> with robust phase correlation (RPC).  $^{24,25}$  In the final PIV pass, an effective interrogation window size of 32 × 32 pixels with an 8 x 8-pixel grid size was used. This resulted in velocity fields of size 127 x 127 vectors. For all PIV passes, a

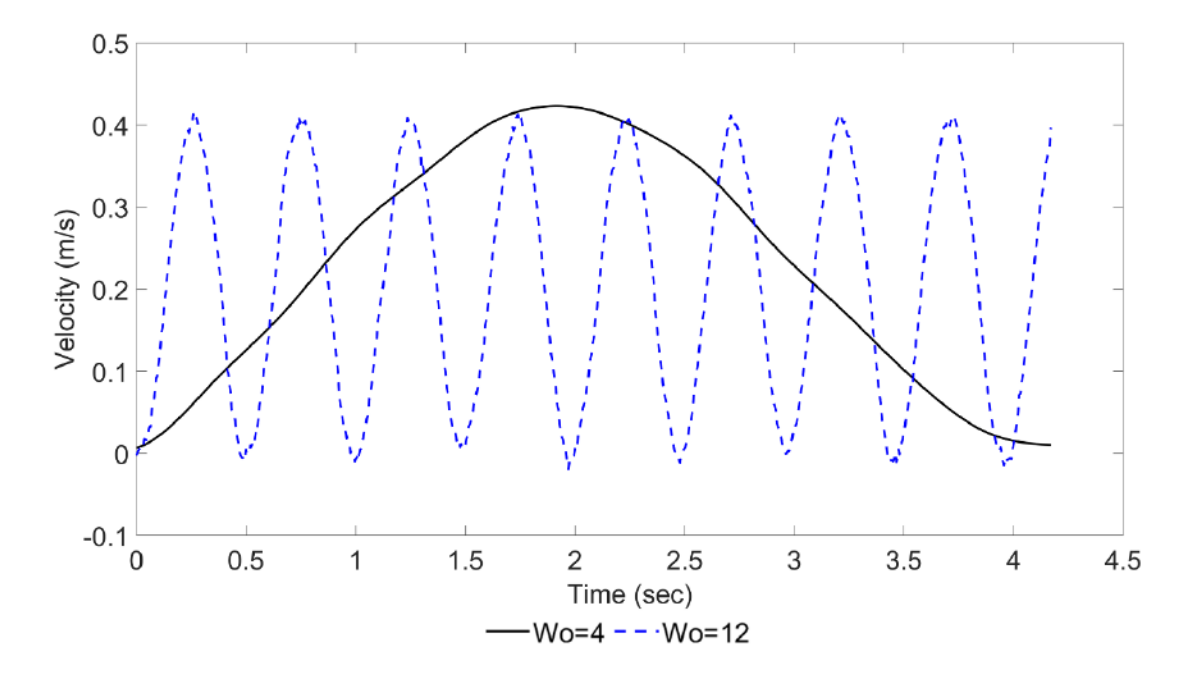


Figure 2 Inflow waveform for mean Reynolds number cases of 800 at 4 and 12 Womersley number.

50% Gaussian window was employed  $^{26}$  to mitigate spectral leakage. For the first and second PIV passes, validation was performed using three median-based universal outlier detection (UOD) passes with window sizes of  $7 \times 7$ ,  $5 \times 5$ , and  $3 \times 3$ , and thresholds of 3, 2, and 2 for the first, second, and third pass, respectively.  $^{27}$  No validation was performed for the final PIV pass.

The velocity fields were filtered using proper orthogonal decomposition (POD)<sup>28</sup> with the autonomous entropy line-fit (ELF) thresholding criterion. <sup>29</sup> POD is commonly used to smoothen PIV velocity fields by decomposing the velocity into a set of eigenmodes and reconstructing a reduced-order representation of the data which discards modes contributed primarily by noise. The ELF thresholding criterion has been shown to provide excellent separability of physical vs. noisy modes even for modes with similar energy contribution. Hence, using the ELF method as compared to traditional energy

thresholding approaches yields a higher fidelity turbulence spectrum, which is particularly important for the goals of this work.<sup>29</sup> Table 2 provides the number of modes and corresponding percent energy retained for each test case. It is important to note that per the ELF criterion, the retained modes are not necessarily the N most energetic modes, but rather the N modes most likely to contain physical flow information. While POD provides good smoothing, it can at times retain outlier vectors. Thus, two final UOD passes were applied to the POD-filtered velocity fields, and the velocity fields were then phase-averaged. For all cases, only two pulsatile cycles were used for phase-averaging. Even though some cases captured additional cycles, utilizing a different number of cycles for the phase-averaging would generate variable smoothing across cases which would introduce bias errors in the fluctuating velocity, TKE, and TI calculations. The phase-averaged velocity fields were then temporally sub-sampled to the temporal resolution of the 12 Womersley number (i.e., the Womersley number with the lowest snapshots per pulsatile cycle). This ensured that all cases maintained the same number of temporal snapshots per pulsatile cycle, thus mitigating resolution-based biases. The smoothed, phase-averaged, and sub-sampled velocity fields (i.e., "filtered PIV velocity") were used for all subsequent calculations.

The Reynolds decomposition was used to compute the fluctuating velocity components according to:

$$u'_{i}(t) = U_{i}(t) - \langle U(t) \rangle \tag{3}$$

where  $u'_i(t)$  is the fluctuating velocity,  $U_i(t)$  is the filtered PIV velocity,  $\langle U(t) \rangle$  is the mean velocity, and t is time. As done in Brindise and Vlachos (2018), <sup>29</sup> the mean velocity was computed using the discrete wavelet transform (DWT). Specifically, for each spatial point, the DWT of  $U_i$  was computed and  $\langle U \rangle$  was defined as the reconstruction of the fifth-level approximate coefficients. Brindise and Vlachos (2018) reported this approach provided as good or better accuracy than a traditional ensemble averaging approach. Moreover, because only 2–40 cycles captured for each test case herein, a traditional ensemble averaging was not possible.

Table 2. Number of POD modes (out of 11,851 snapshots) and the corresponding energy retained for each test case.

$Re_m/Wo$	Number of saved modes	Corresponding energy
$800Re_m$ 4Wo	1489	99.681
$800Re_m$ 12Wo	1134	98.988
$2300Re_m$ 4Wo	732	96.717
$2300Re_m$ 6Wo	635	97.292
$2300Re_m$ 8Wo	767	96.503
$2300Re_m$ 10Wo	786	96.773
$2300Re_m$ 12Wo	891	95.736
$2500Re_m$ 4Wo	880	97.267
$2500Re_m$ 12Wo	752	96.209
$2700Re_m$ 4Wo	923	96.659
$2700Re_m$ 6Wo	1195	97.161
$2700Re_m$ 8Wo	1268	95.772
$2700Re_m$ 10Wo	1298	96.221
$2700Re_m$ 12Wo	1248	95.656
$3200Re_m$ 4Wo	766	93.258
$3200Re_m$ 12Wo	806	93.708
$4200Re_m$ 4Wo	685	90.992
$4200Re_{m}$ 12Wo	977	93.352

Equations (4) and (5) were used to calculate TKE and TI, respectively,

$$k(t) = \frac{1}{2}(u'(t)^2 + v'(t)^2), \tag{4}$$

$$I(t) = \frac{1}{u_c(t)} \sqrt{\frac{1}{2} (u'(t)^2 + v'(t)^2)},\tag{5}$$

- 4 where K is the TKE  $(m^2/s^2)$ , I is the TI (%),  $u_c$  is the centerline velocity (m/s). As introduced by Trip et
- 5 al (2012)<sup>15</sup>, and used in Brindise and Vlachos (2018), the effect of pump fluctuations on the TKE and TI
- 6 calculations was minimized by subtracting the axial line average fluctuating velocity from each  $u'_i(t)$
- 7 velocity field.

- Phase lag between the TI-inflow waveform velocity and TI-inflow waveform acceleration were
- 9 computed by first smoothing the TI, velocity, and acceleration waveforms. A sine wave was then fit to

- each smoothed waveforms. Phase lag was defined as the difference between the temporal position of the
- 2 TI peak and the velocity/acceleration peak in the fitted sine wave and was normalized by cycle length.
- 3 The sine wave fitting method prevented potential errors caused by spikes and intermittency in the TI
- 4 waveform. Additionally, because a sine wave was used as the input flow waveform, it provides an
- 5 appropriate fitting function.

- 6 Coherent structures were identified using the  $\lambda_{ci}$  criterion, 30 which computes the relative vortex
- 7 strength as the maximum imaginary portion of the spatial velocity gradient eigenvalues.

#### 3 Results and Discussion

#### A. Effect of Womersley number on turbulent structure development

We first evaluated the velocity profiles to confirm the experimental setup maintained sufficient consistency across test cases. Additionally, the temporal and spatial development of the coherent structures were investigated to explore how Womersley number affected the development of transitional and turbulent flow.

Figure 3 illustrates the temporally and axially averaged velocity profiles for all Womersley number cases at each mean Reynolds number. The analytical Poiseuille flow solution is also plotted for reference with the 800 mean Reynolds number case. For each mean Reynolds number case, good agreement is observed across Womersley numbers, confirming the consistent and fully developed flow characteristics of the experimental setup. The median of the point-by-point difference between the Poiseuille flow profile and the experimental flow profile of the 800 mean Reynolds number, 4 and 12 Womersley number cases was 5.6% and 3.1%, respectively. This suggests—as expected—that the flow for these cases is laminar. For mean Re cases of 2300, 2500, and 2700, the core region shows an increasingly uniform core region profile and higher wall gradients. This highlights that the flow is transitional by a mean Re of 2300 and the development of turbulence is increasing as Reynolds number increased to 2700. By a mean Re of 3200, the velocity profile strongly resembles a fully turbulent one.

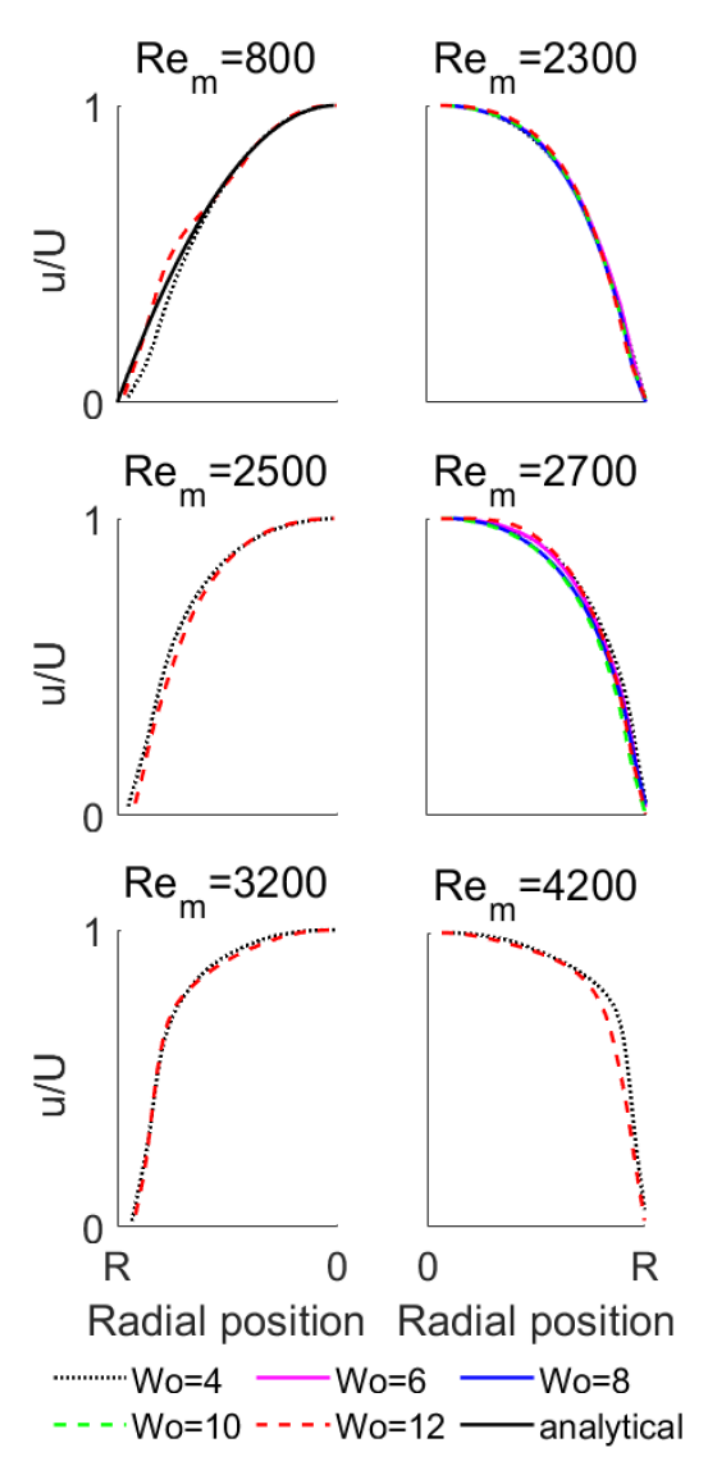


Figure 3. Axially and temporally averaged velocity profiles for all cases. for 800 mean Reynolds number cases, the analytical Poiseuille solution is plotted.

- 1 Moreover, the mean Re cases of 3200 and 4200 maintained the same velocity profiles, suggesting that
- 2 both cases are fully turbulent.

To explore the dynamics and formation of flow instabilities and turbulent structures with increasing mean Reynolds number, Figure 4 shows the coherent structures at the cycle point corresponding to the peak flow rate for all mean Reynolds number cases at 4 and 12 Womersley numbers. The generalized behavior of the coherent structures was similar for both Womersley numbers. For the 2300, 2500, and 2700 mean Reynolds number cases, coherent structures were increasingly observed in the core flow region. At mean Reynolds numbers of 3200 and 4200, turbulent structures with larger swirl strength were present in the near wall region. Additionally, these cases maintained larger coherent structures in the core flow than were observed in the lower mean Re cases. The lack of coherent structures in the core flow region for the lower mean Re cases suggests that the turbulent structures developed in the near wall regions were dissipated in that region. However, with increasing mean Re, the structures are formed faster than they can be dissipated, and structures are swept into the core flow. This notion agrees with the findings of Brindise and Vlachos (2018) and He and Jackson (2009) who both reported that when turbulence production exceeds the rate of turbulence dissipation in the near wall region, pressure waves transport turbulent structures to the core flow, increasing the overall turbulence of the flow. 10,19 Considering the role of Womersley number more closely, differences between the strength and shape of the coherent structures were observed between the 4 and 12 Womersley number. Specifically, the 12 Womersley number case maintained on average 25.2% and 9.0% higher swirl strength than the 4 Womersley number case at mean Reynolds numbers of 3200 and 4200, respectively. Further, the structures in the core flow for the 4200 mean Reynolds number case (e.g. structures within the orange circles) were qualitatively larger in the 4 Womersley number case than the 12 Womersley number case. However, the number of structures observed at peak flow rate for the 4 and 12 Womersley numbers was similar. Together, these findings suggest that Womersley number affected the shape and size of the turbulent structures, particularly in the core flow.

1

2

3

4

5

6

7

8

9

10

11

12

13

14

15

16

17

18

19

20

21

22

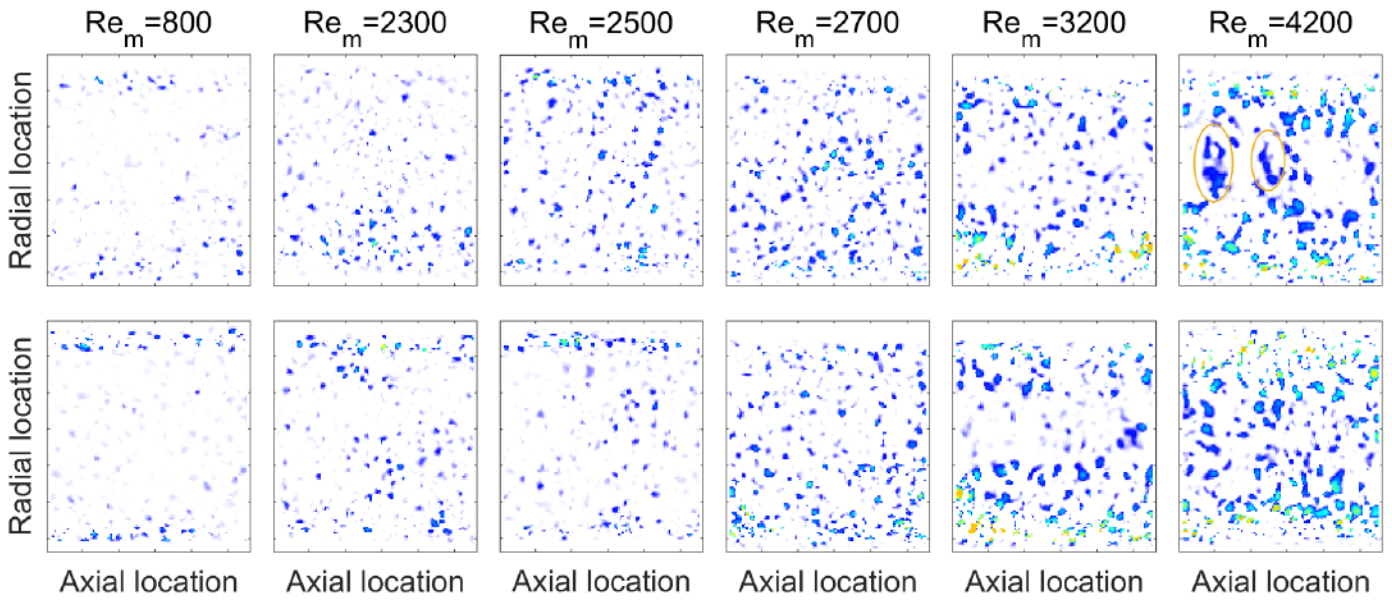


Figure 4. Coherent structures for all mean Reynolds numbers at Womersley numbers of 4 and 12. The contours represent the  $\lambda_{ci}$  value, indicating the relative strength of the coherent structure.

Figure 5 explores the temporal development of turbulence through the pulsatile cycle. Specifically, Figure 5 shows the coherent structures at mid-acceleration, peak flow rate, and mid-deceleration for the 800, 2700, and 4200 mean Reynolds number cases, each at 4 and 12 Womersley number. For the mean Reynolds number of 800, significant differences in the coherent structures at mid-acceleration, peak flow rate, and mid-deceleration were observed across Womersley numbers. At 4 Womersley number, no coherent structures were present during the mid-acceleration and mid-deceleration time steps, while at 12 Womersley number, coherent structures primarily localized in the wall region were clearly observed. The flow instabilities formed at peak systole in the near wall region are caused by the high shear gradients at the wall (as compared to the core region). Oherent structures are increasingly observed in the core flow region as the mean Reynolds number is increased to 2700 and 4200. At the 2700 mean Reynolds number case, larger coherent structures were observed at mid-acceleration and mid-deceleration for the 4 Womersley number. Additionally, for the 4200 mean Reynolds number case at mid-acceleration, the 12 Womersley number maintained notably more structures in the core flow than the 4 Womersley number. In the core flow at mid-deceleration, the 12 Womersley number is observed to maintain structures with higher swirl strength, while the 4 Womersley number maintains larger sized structures.

These findings suggest that the large coherent structures observed in low Womersley numbers are broken down to smaller and higher swirl strength coherent structures at high Womersley numbers. At such high Womersley number, there is insufficient time to allow structures travel to the core region, so more coherent structures remain in the near wall region where high shear gradients lead to higher swirl strength and eventually breaking down of structures. This notion aligns with the observation in Xu and Avila (2018)<sup>16</sup> that smaller turbulent structures analogous to steady flow structures occur in higher Womersley number flows. Additionally, these results show that coherent structures at 12 Womersley number did not change significantly throughout the pulsatile cycle. This highlights that at the 12 Womersley number the development of coherent structures was largely independent of the pulsatility while at the 4 Womersley number, the coherent structure formation was influenced by the unsteady flow waveform. This expands on findings of Scotti and Piomelli (2001)<sup>11</sup> and He and Jackson (1986)<sup>10</sup> who reported that for turbulent flows, high pulsation frequency yields insufficient response time for the flow to be affected by the

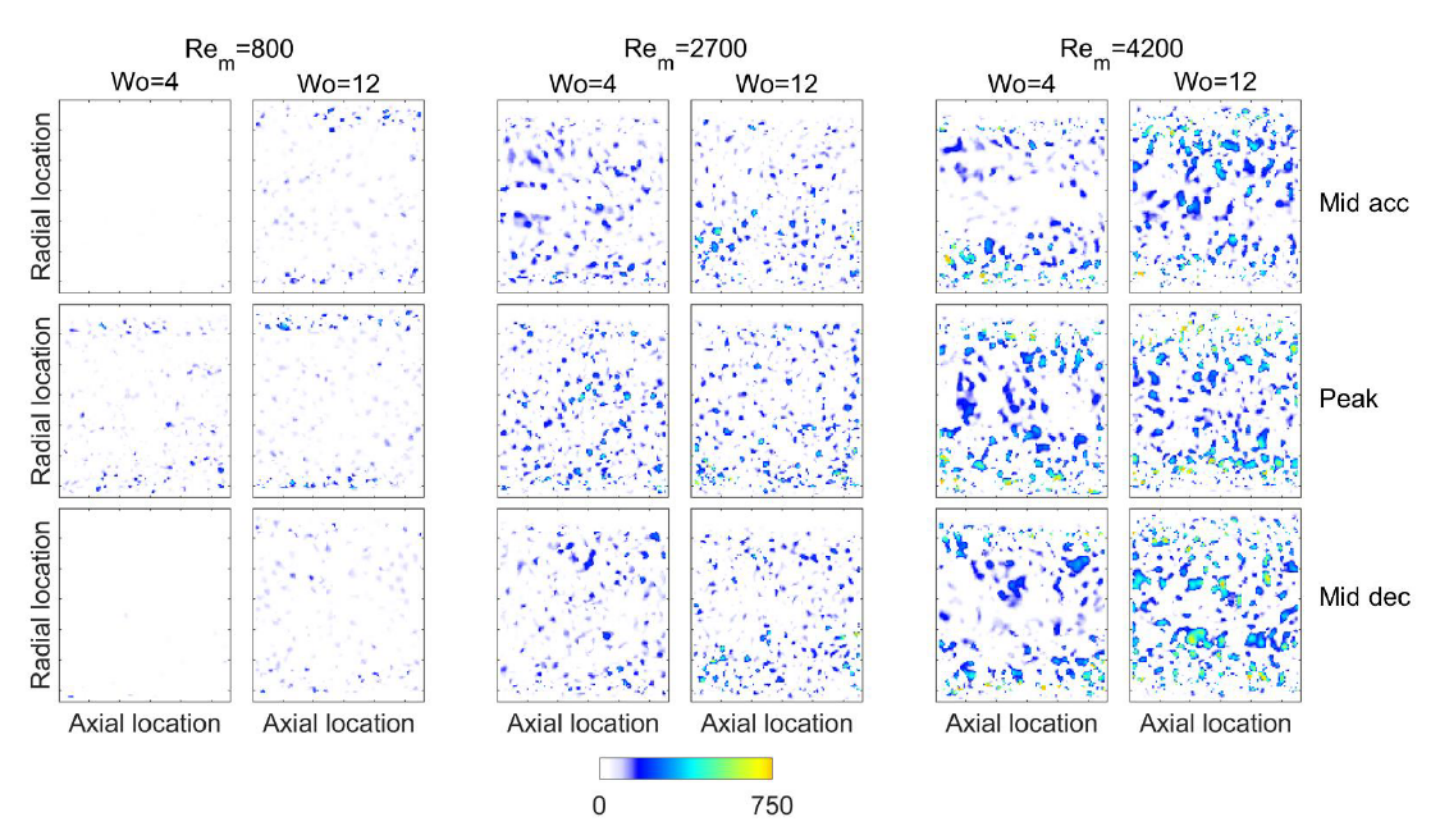


Figure 5 Coherent structures for 800, 2700, and 4200 mean Reynolds numbers at Womersley numbers of 4 and 12 during mid acceleration, peak, mid declaration. The contours represent the  $\lambda$ ci value, indicating the relative strength of the coherent structure.

- 1 pulsatility. Specifically, our results suggest that for laminar, transitional, and turbulent flows, the exists
- a "critical Womersley number" beyond which the flow becomes independent of pulsatility.

3

4

5

6

7

8

9

10

11

12

13

14

15

16

17

18

19

20

21

22

23

24

### B. Exploring the effect of Womersley number on TKE, TI, and critical Reynolds number

We next evaluated how Womersley number affected turbulence metrics and the observed critical Reynolds number. Figure 6 shows the temporally and spatially averaged TKE for all mean Reynolds number cases as a function of Womersley number. At 4 Womersley number, average TKE was 5.8e-6  $m^2/s^2$ , 1.5e-5  $m^2/s^2$ , 2.9e-5  $m^2/s^2$ , 4.2e-5  $m^2/s^2$ , 1.6e-4  $m^2/s^2$ , and 2.0e-4  $m^2/s^2$  for the mean Reynolds number cases of 800, 2300, 2500, 2700, 3200, and 4200, respectively. Hence, between mean Reynolds numbers of 800 to 2700, a gradual increase of average TKE was observed, followed by an exponential upsurge in average TKE between the 2700 and 3200 mean Reynolds number and subsequently a moderate increase going to the 4200 mean Reynolds number. These results indicate that flow remained in the transitional regime for mean Reynolds number cases between 2300 and 2700 and was fully turbulent by mean Reynolds number of 3200. This suggests that the bulk of the transitional phase for this setup occurs in the Reynolds number range of 2700 and 3200. Meanwhile, average TKE at 12 Womersley number was  $8.9e-6 \text{ m}^2/\text{s}^2$ ,  $2.0e-5 \text{ m}^2/\text{s}^2$ ,  $1.3e-5 \text{ m}^2/\text{s}^2$ ,  $4.7e-5 \text{ m}^2/\text{s}^2$ ,  $1.8e-4 \text{ m}^2/\text{s}^2$ , and  $2.1e-4 \text{ m}^2/\text{s}^2$  for the mean Reynolds number cases of 800, 2300, 2500, 2700, 3200, and 4200, respectively. Hence, on average TKE was about 11% higher at 12 Womersley number than at 4 Womersley number for each Reynolds number case. Similar to the 4 Womersley number cases, for the 12 Womersley number case, average TKE was observed to steadily increase with increasing mean Reynolds number, with transition again expected to occur between 2700 and 3200. Moreover, the observed trend of increasing average TKE with increasing Womersley number suggests that the overall fluctuating component in the flow was proportional to Womersley number. Therefore, we find that at higher Womersley numbers disturbed flow components are more dominant. This is consistent with the findings in Figure 5 where we observed more coherent structure with larger swirl strength across the cycle at the 12 Womersley number cases.

To investigate the critical Reynolds number, Figure 7 illustrates the spatially and temporally averaged TI plotted against the mean Reynolds number. It is important to note that our experimental setup was not rigorously controlled enough to determine specific critical Reynolds number values. Thus, the results presented here should be considered only for the trends across cases that they show. At a 4 Womersley number, the average TI was 1.03%, 0.77%, 1.00%, 1.12%, 2.01%, and 1.89% for the mean Reynolds number cases of 800, 2300, 2500, 2700, 3200, and 4200, respectively. Meanwhile, average TI at 12 Womersley number was 1.28%, 0.96%, 0.64%, 1.23%, 2.20%, 1.99% for the mean Reynolds number cases of 800, 2300, 2500, 2700, 3200, and 4200, respectively. The 12 Womersley number cases on average maintained a 15% higher average TI for all mean Reynolds number than the 4 Womersley number cases. In general, the critical Reynolds number is observed to occur around a mean Reynolds number of 3000 for both the 4 and 12 Womersley number cases. While for Womersley numbers of 6, 8, and 10 only data for mean Reynolds numbers of 2500 and 2700 was available, these TI values closely

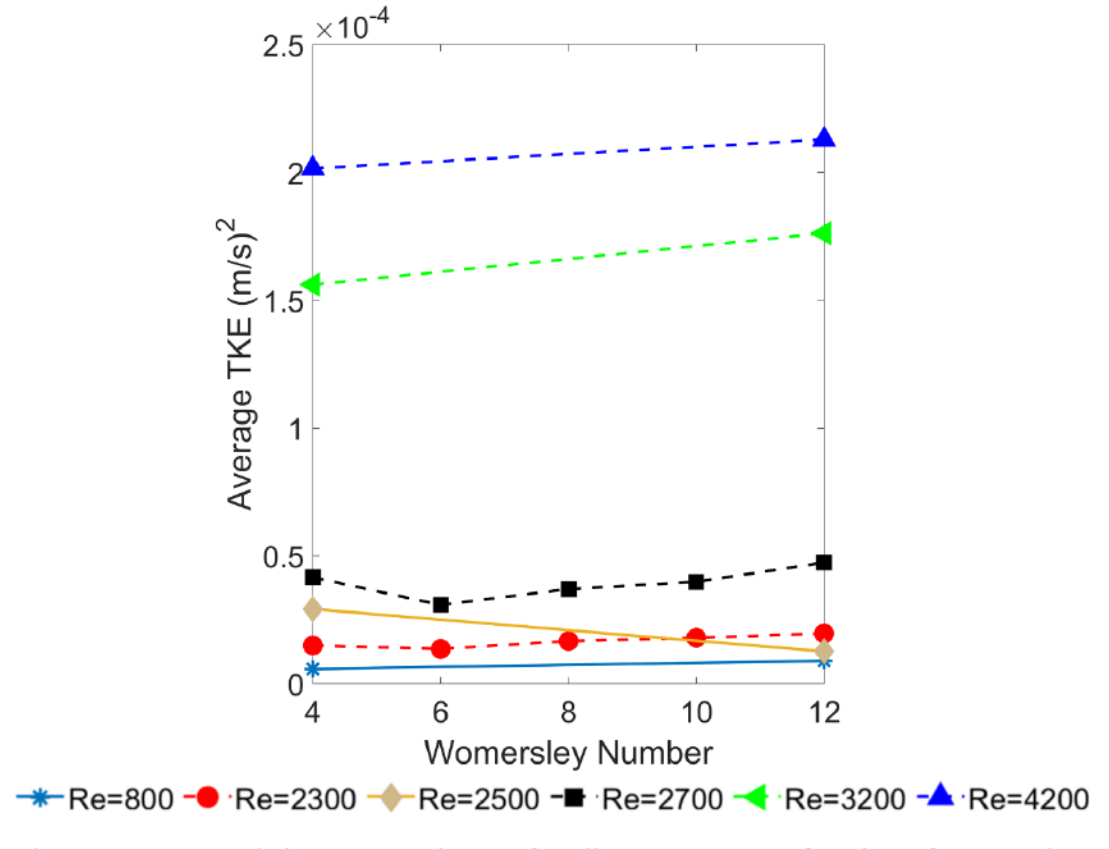


Figure 6. Space and time averaged TKE for all test cases as a function of Womersley number.

follow the 4 and 12 Womersley number cases. Figures 6 and 7 suggest that critical Reynolds number wasn't significantly affected by Womersley number for the tested range of values. However, because our study cannot exactly pinpoint the critical Reynolds number without employing an interpolating s-curve fit, this should be explored further in future work. Nonetheless, our results show that although Womersley number was shown to affect the dynamics and development of transition and turbulent structures, this did not precipitate an appreciable change in critical Reynolds number. This finding agrees with previous studies which reported critical Reynolds number is independent of Womersley number at 'high' Womersley numbers (Wo≥10). 15-18 However, contradictions arise with other studies that found critical Reynolds number to decrease as Womersley number increased through the 'intermediate range' (4≤Wo≤10). 16-18 Additionally, at 'low' Womersley numbers (Wo≤4) both a decrease 18 and a null effect have been reported. 16,17 We speculate that the reported inconsistencies could be caused in part by differences in perturbation methods. For example, Stettler & Hussain (1986) and Trip et al. (2012) used orifice plates, 15,18 while Xu et al. (2017) and Xu and Avila (2018) 16,17 used impulsive perturbations. No active perturbations were introduced to the flow in this study. It is plausible that this added source of turbulence may lower the Womersley number at which transition begins to mimic steady flow and possibly explain, in part, the different effect of Womersley number on critical Reynolds number across varying study designs. Moreover, Xu and Avila (2018) found pulsation amplitude to affect the critical Reynolds number. They defined pulsation amplitude as  $A = U_0/U_s$ , where  $U_0$  is the oscillatory component of the speed and U<sub>s</sub> is the mean speed. By this definition, the pulsation amplitude wasn't constant in our study, but rather decreased with increasing Reynolds number. Thus, according to their findings, our critical Reynolds number should have increased with increasing amplitude of pulsation. However, due to our study design, the decrease in pulsation amplitude was accompanied with an increase in mean Reynolds number. Although this could have accelerated the occurrence of transition in our setup, this wouldn't change the observed trends regarding the effect of Womersley number. Therefore, the isolated effect of pulsation amplitude should be explored in future work. Additionally, Peacock et.al (1998), who reported a monotonic increase in critical Reynolds number across Womersley numbers ranging from 4-

1

2

3

4

5

6

7

8

9

10

11

12

13

14

15

16

17

18

19

20

21

22

23

24

25

20,<sup>2</sup> employed large pulsation amplitudes and didn't introduce active perturbation to the flow in their experiment, similar to our study. The discrepancies reported in our study and in Peacock et al. (1998) further suggest that pulsation amplitude and the used perturbation methods may both affect the critical Reynolds number and the specific role of these factors should be further explored in future work. Although critical Reynolds number was independent of Womersley number, the analysis of coherent structures along the cycle in transitional flow has shown that the size, number, and swirl strength of coherent structures are affected by Womersley number. Therefore, we next explore the temporal trends of TKE/TI to provide further insight on the effect of Womersley number on development of transition throughout the pulsatile cycle.

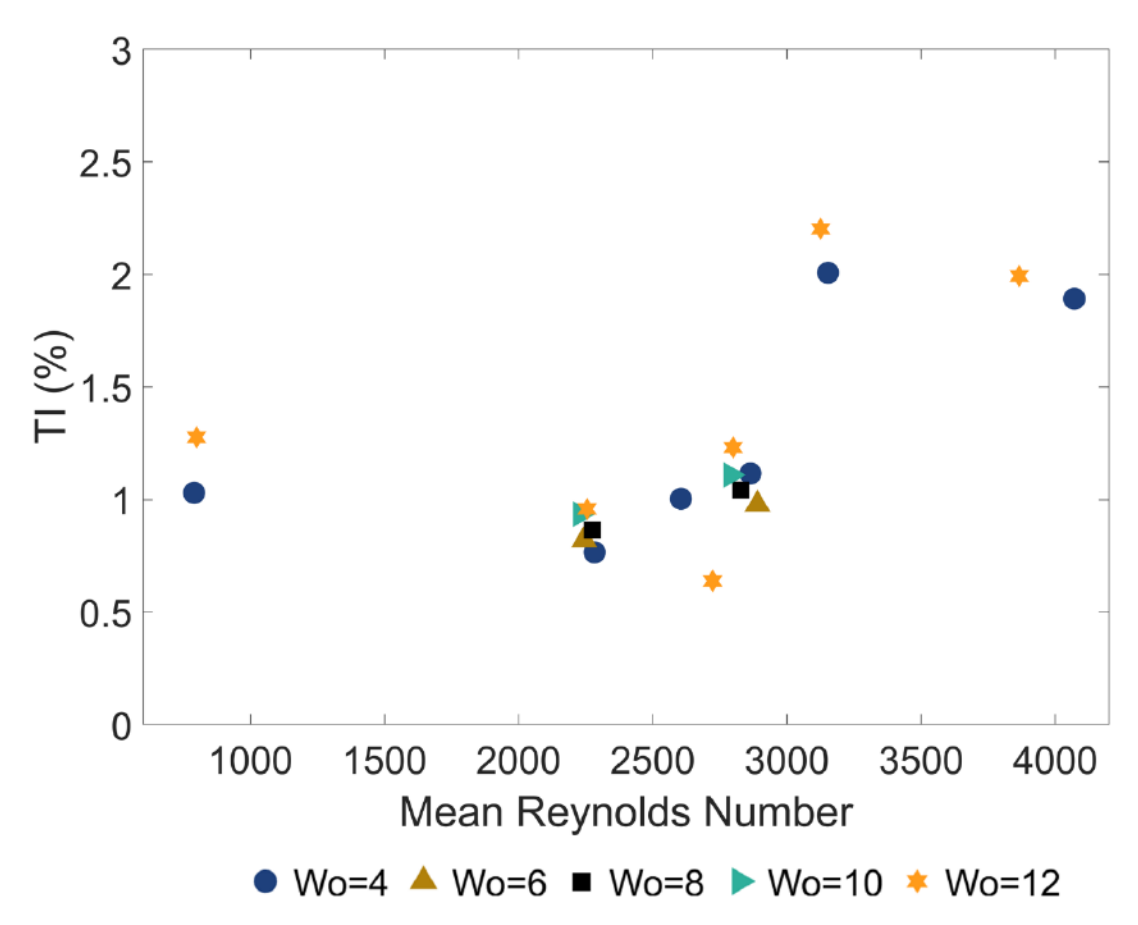


Figure 7. Spatiotemporally averaged TI for all test cases as a function of mean Reynolds number.

We next consider the temporal variation of the TKE and TI trends throughout the pulsatile cycle. Figure 8 shows the spatially averaged TI and TKE vs. time trends. TKE was normalized by the mean

TKE for each case. For the 800 mean Reynolds number cases, TI was not defined at the beginning and end of the cycle because the velocity waveform (and therefore centerline velocity) went to zero. For the 4 Womersley number case, a spike in TKE and TI is observed at t/T of about 0.82 for the 2300 mean Reynolds number which suggests the burst of a turbulent puff<sup>31</sup> during the deceleration portion of the cycle. As the mean Reynolds number is increased to 2500, intermittent spikes in both TKE and TI are observed during the deceleration phase starting at a t/T of about 0.62 which suggests the beginning of the transitional regime. By 2700 mean Reynolds number, intermittent spikes in TKE and TI are observed at the start of the cycle but dissipate as the flow accelerates. Intermittency and spikes appear again during the deceleration phase. The dynamics observed during the acceleration and deceleration phases agree with previous studies that reported turbulence relaminarizes during the acceleration period and is largely produced during the deceleration phase which maintains an adverse pressure gradient.<sup>13,15,18</sup> The 3200 and 4200 mean Reynolds numbers maintained consistent fluctuations throughout the pulsatile cycle, highlighting that the flow was fully turbulent by this point. The 12 Womersley number maintained significant differences in the dynamics. Specifically, the intermittent TKE and TI spikes were smaller in magnitude and distributed throughout the pulsatile cycle rather than being localized in the deceleration phase. These findings—consistent with Figure 5—suggest that the 12 Womersley number case yielded smaller turbulent puff structures that were agnostic to the underlying pulsatile flow dynamics (i.e., transition is no longer phase dependent). This also suggests that a high frequency of pulsation minimizes the effect of parameters like waveform shape on the development and occurrence of transition. This notion should be explored in future work.

1

2

3

4

5

6

7

8

9

10

11

12

13

14

15

16

17

18

19

20

21

22

23

24

25

To explore this notion that the flow became independent of the pulsatile phase further, in Figure 9 the interquartile range (IQR) of the normalized spatially-averaged temporal TKE trends (i.e., the lines plotted in Figure 8) is plotted as a function of mean Reynolds number. The IQR provides a relative measure of the pulsatility observed in the TKE trend such that a high IQR indicates the TKE trend maintained a pulsatile trend, while a low IQR indicates the TKE trend was more constant throughout the

pulsatile cycle. For the 4 Womersley number, the IQR was high for the 800 mean Reynolds number and generally decreased with increasing mean Reynolds number. For example, at a mean Reynolds number of 800, the 12 Womersley number case maintained a 67% lower TKE IQR than the 4 Womersley number. By a mean Reynolds number of 4200, the TKE IQR of the two Womersley numbers was significantly closer. Specifically, while the two Womersley numbers maintained opposite trends with increasing mean Reynolds number, they appeared to generally converge to a similar IQR value. These findings highlight

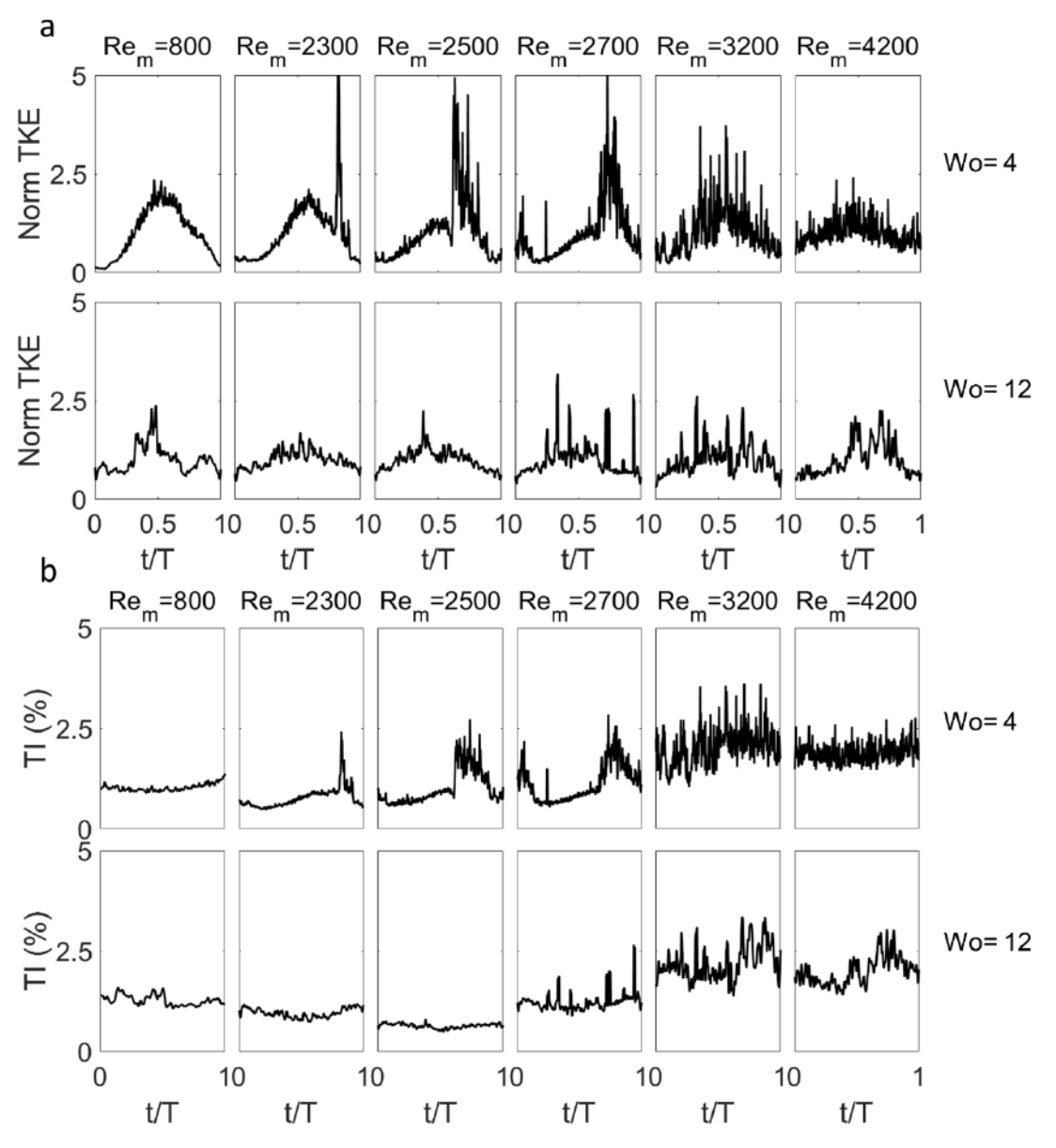


Figure 8. Spatially averaged TKE(A) and TI(B) through time for all mean Reynolds number cases at 4 and 12 Womersley number.

that for the 12 Womersley number case the TKE trend was largely unaffected by the pulsatility at any mean Reynolds number and the increase in IQR range is attributed solely by the increase in turbulent energy. This confirms that the 12 Womersley number case resembled steady flow dynamics. Additionally, these findings indicate that the magnitude of fluctuations induced by fully turbulent flow seem to be independent of Womersley number. For the Womersley numbers of 6 and 8, the TKE IQR is observed to decrease with increasing Reynolds number, similar to the 4 Womersley number. Meanwhile, the 10 Womersley number TKE IQR increased with increasing mean Reynolds number. This suggests that the Womersley number where the transitional flow begins to mimic steady flow occurs in the 8–10 Womersley number range. However, because only two mean Reynolds numbers were tested for the 6, 8, and 10 Womersley numbers, this observation should be interpreted with caution.

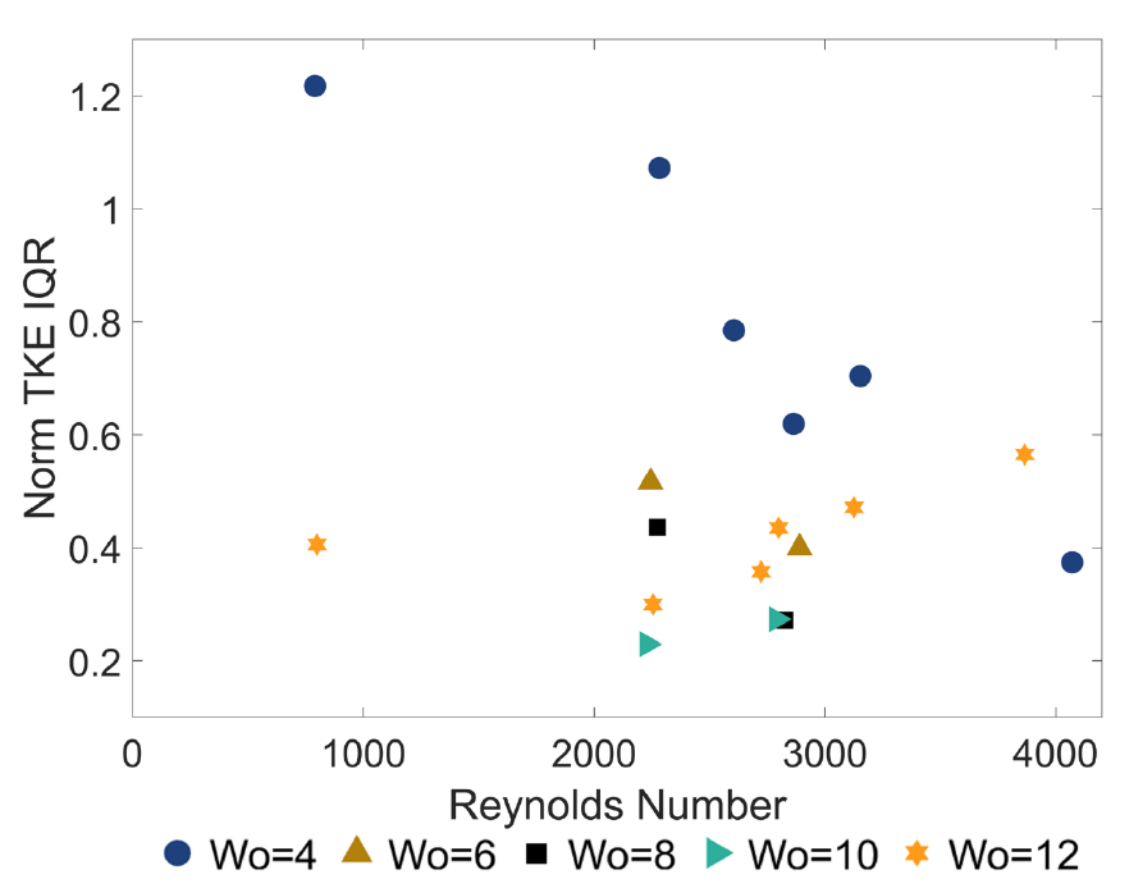


Figure 9. Interquartile range of spatially averaged TKE through time for all cases as a function of mean Reynolds number

#### C. Investigating the TI-input waveform phase lag as a function of Womersley number

1

2

3

4

5

6

7

8

9

10

11

12

13

14

15

16

17

18

19

20

21

22

23

24

25

Figure 8 demonstrates that a phase lag between the TI and inflow velocity waveform existed. Specifically, for several cases, it is clearly observed that the minimum TI occurs at about a t/T of 0.5, when the velocity waveform is at peak flow rate. Moreover, the loss of influence of the pulsatility on TKE trends as shown in Figure 9 suggests that the TI-velocity phase lag may change as the flow dynamics change with increasing Womersley number. In such a case, it is plausible that the TI-velocity phase lag may capture underlying dynamics of pulsatile transition. Therefore, in Figure 10, the phase lag of TIvelocity and TI-acceleration was plotted as a function of the mean Reynolds number. Due to the aforementioned challenges for calculating TI for the 800 mean Reynolds number cases, phase lag for these cases couldn't be reliably computed and wasn't included in this analysis. For the 4 Womersley number, phase lag steadily decreased with increasing mean Reynolds number, a trend matching that observed with the TKE IQR range. The total decrease of phase lag from 2300 to 4200 mean Reynolds number was 83.7% and 35.2% for TI-velocity and TI-acceleration, respectively. For the 12 Womersley number cases, phase lag increased with increasing mean Reynolds number by a total of 33% and 22% for TI-velocity and TI-acceleration, respectively. In general, the TI-velocity and TI-acceleration waveforms closely matched each other for all Womersley numbers. In this study a sinusoidal waveform was used such that the acceleration and deceleration gradients mirrored each other; it would be of interest to explore in future work if the TI-velocity and TI-acceleration phase lags differ for cases were the inflow waveforms maintained varying average acceleration-to-deceleration gradient ratios.

Figure 10 highlights that each Womersley number maintained its own unique phase lag trend. Thus, in Figure 11 the phase lag averaged across all mean Reynolds numbers for each Womersley number is plotted as a function of Womersley number. Results from previous studies (Trip et al. (2012) and Brindise and Vlachos (2018)) were plotted as well. (For Brindise and Vlachos (2018), only the Symmetric waveform data was used since this closely matches a sinusoidal waveform.) Averaged TI-vel phase lag was -43° (Brindise and Vlachos, 2018),  $-107^{\circ} \pm -25^{\circ}$ ,  $-146^{\circ} \pm -3.1^{\circ}$ ,  $-175^{\circ} \pm -16.5^{\circ}$ ,  $-165^{\circ} \pm -27^{\circ}$ ,  $-168^{\circ} \pm$ 

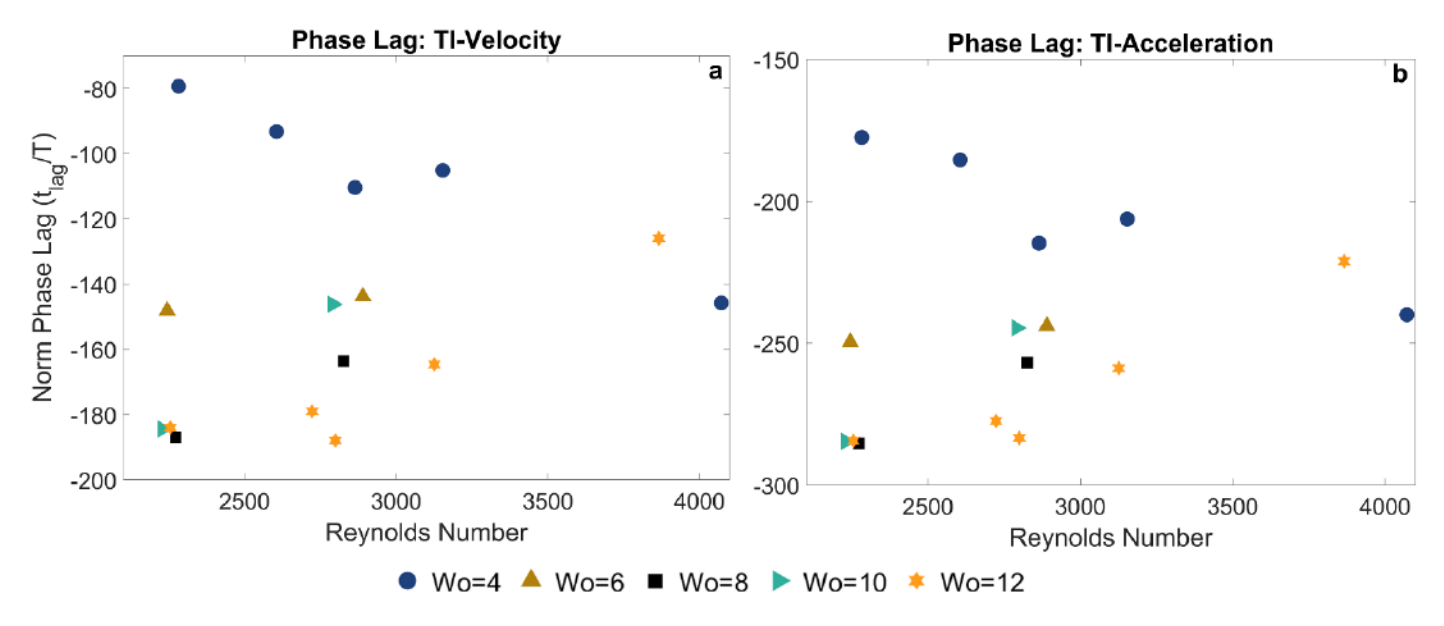


Figure 10. Phase lag of TI-velocity and TI-acceleration vs Reynolds number.

1

2

3

4

5

6

7

8

9

10

11

12

13

14

15

16

25°, and -180° (Trip et al., 2012) at Womersley numbers of 2.4, 4, 6, 9, 10, 12, and 15, respectively. Averaged TI-acceleration phase lag was -144° (Brindise and Vlachos, 2018), -205° ± 25°, -247° ± 3.1°, - $271^{\circ} \pm 16.5^{\circ}$ ,  $-265^{\circ} \pm 27^{\circ}$ ,  $-265^{\circ} \pm 25^{\circ}$ ,  $-270^{\circ}$  (Trip et al., 2012) at Womersley numbers of 2.4, 4, 6, 9, 10, 12, and 15, respectively. As Womersley number increased from 4 to 8, the average phase lag dropped by 321% and 89% for TI-velocity and TI-acceleration, respectively. However, as Womersley number increased from 8 to 15, phase lag only varied by about 7% and 3% for TI-velocity and TI-acceleration, respectively. Therefore, a trend is observed in which TI-velocity and TI-acceleration phase lags decrease then plateau at Wo=8. It is observed that the included prior studies of Trip et al. (2012) and Brindise and Vlachos (2018) both agreed with and extended the trend established by our data (including the plateau phase lag value). This is particularly of interest given that these two studies used notably different amplitudes of oscillation as compared to our study. Hence, this provides evidence suggesting that phase lag may provide a universal indication of the influence of Womersley number on the transitional flow. Moreover, this plateau may indicate that the Womersley number of 8 is the changepoint above which transition becomes largely independent of Womersley number and steady flow dynamics are recovered. By extension, this would suggest that—for our setup—a Womersley number of 8 represents the point where flow has insufficient response time for dissipation as a result of the high frequency of pulsation (and low cycle time), as detailed by Scotti and Piomelli (2001). (It would be of interest to consider in future work if this "critical" Womersley number is altered if active perturbations are added to our setup which may induce an insufficient response time at a lower Womersley number.) Given this, it is plausible that the phase-lag evaluation may indirectly characterize the relationship between turbulence dissipation and production. This is a notion that should be explored in future work which explicitly evaluates the TKE budget.

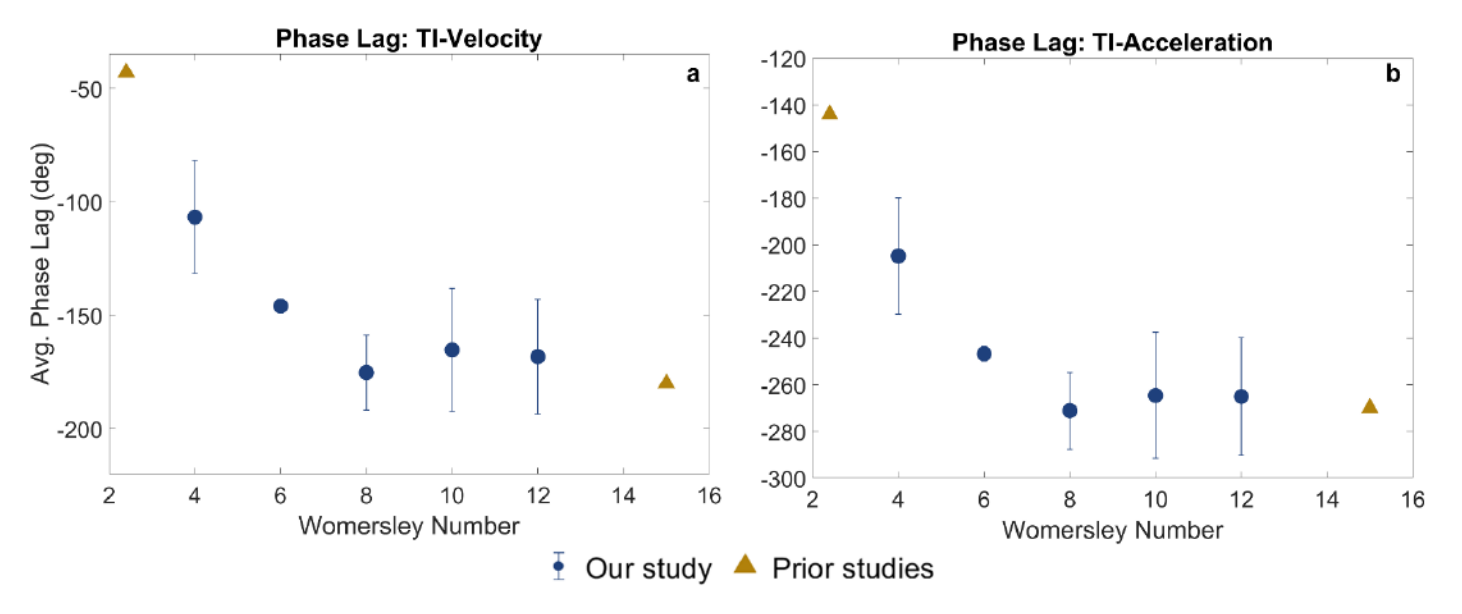


Figure 11. Phase lag of TI-velocity and TI-acceleration vs. Womersley number. Phase lag at Wo=3 reported by Brindise and Vlachos <sup>19</sup>, phase lag at Wo=15 reported by trip et.al<sup>15</sup>

#### D. Limitations

Several limitations of our study existed. The computer-controlled gear pump used in this setup introduced fluctuations into the flow. This made it challenging to produce a clean well controlled sinusoidal input waveform with a Womersley number larger than 12. These fluctuations can be mitigated by implementing a flow straightener into the flow loop which should be considered in future studies. Moreover, limitations to the PIV camera's onboard RAM memory limited the data capture to only two cycles for the 4 Womersley number cases. Thus, this limited the phase averaging for all cases with higher Womersley numbers to using only two cycles as well in order to have comparable results. Additionally, steady state cases weren't tested in this study such that comparisons between steady flow dynamics and

dynamics at high Womersley number cases (Wo=12) could not be explicitly confirmed for our setup. For our setup, the critical Reynolds number was slightly higher than expected. This is because critical Reynolds number is highly dependent on initial conditions and specifications of experimental setup. As a result, the exact critical Reynolds number couldn't be precisely pinpointed as it occurred outside the range of our detailed Reynolds number capture (2300-2700). However, the trends in TKE/TI vs Re were clear and we were able to observe flow develop from laminar to transitional to turbulent throughout the selected range. Thus, despite this limitation, we were able to sufficiently explore the trends and dynamics of transitional flow. Furthermore, because mean Reynolds numbers of 2300 and 2700 fall within the transitional Reynolds number range of interest, Womersley numbers of 6, 8, and 10 were only tested for these two cases. However, testing a finer range of Womersley numbers across more mean Reynolds numbers cases could provide informative details on the trends observed in this study.

### 4 Conclusions

In this study we investigated the effects of Womersley number on transition to turbulence in pulsatile pipe flow. In particular, we focused on evaluating the Womersley number range of 4–12 within which considerable contradictory findings have been reported among prior studies. We observed that higher Womersley number flows produced turbulent puffs with smaller spatial size and larger swirl strength as compared to lower Womersley number flows. Additionally, turbulent structures were to a greater extent observed throughout the pulsatile cycle for the high Womersley number, whereas for the low Womersley number the deceleration phase largely drove the formation of turbulent puffs. The temporal trends of spatially-averaged TKE and TI further supported this finding. This suggests that intermittency and, subsequently, transition occur independently of inflow waveform phase at high Womersley numbers. Analysis of average TKE and TI showed that critical Reynolds was relatively unaffected by Womersley number. We speculate that inconsistencies regarding critical Reynolds number within literature are due to differences in pulsation amplitude and the used perturbation method across experiments. Given the noted differences observed in the influence of pulsatility on TKE and TI trends as a function of

- 1 Womersley number, we evaluated the phase lag between TI-input velocity waveform and TI-input
- 2 velocity acceleration. The phase lag was observed to decrease with increasing Womersley number, until
- 3 a Womersley number of 8 at which point the trend plateaued. This suggests that a Womersley number
- 4 of 8 may serve as a "critical" Womersley number beyond which steady flow dynamics are recovered.
- 5 Moreover, data from two prior studies were included in our phase lag analysis which importantly
- 6 suggested that phase lag may provide a universal indicator of the extent to which Womersley number
- 7 affects transition for a given flow. Future work should explore this significant finding further.

# Acknowledgements

- 9 This study was supported by an American Heart Association (AHA) Career Development Award
- 10 (94035) as well as a National Science Foundation (NSF) grant (Award number 23357

#### References

8

11

- <sup>1</sup> M. Andersson, T. Ebbers, and M. Karlsson, "Characterization and estimation of turbulence-related
- wall shear stress in patient-specific pulsatile blood flow," J Biomech 85, 108–117 (2019).
- <sup>2</sup> J. Peacock, T. Jones, C. Tock, and R. Lutz, "The onset of turbulence in physiological pulsatile flow
- in a straight tube," Exp Fluids **24**(1), 1–9 (1998).
- <sup>3</sup> M.C. Brindise, C. Chiastra, F. Burzotta, F. Migliavacca, and P.P. Vlachos, "Hemodynamics of Stent
- 18 Implantation Procedures in Coronary Bifurcations: An In Vitro Study," Ann Biomed Eng 45(3), 542–
- 19 553 (2017).
- <sup>4</sup> S. Morlacchi, S.G. Colleoni, R. Cárdenes, C. Chiastra, J.L. Diez, I. Larrabide, and F. Migliavacca,
- 21 "Patient-specific simulations of stenting procedures in coronary bifurcations: Two clinical cases," Med
- 22 Eng Phys **35**(9), 1272–1281 (2013).

- <sup>5</sup> K.M. Saqr, S. Tupin, S. Rashad, T. Endo, K. Niizuma, T. Tominaga, and M. Ohta, "Physiologic
- 2 blood flow is turbulent," Sci Rep **10**(1), 15492 (2020).
- <sup>6</sup> K. Valen-Sendstad, K.-A. Mardal, M. Mortensen, B.A.P. Reif, and H.P. Langtangen, "Direct
- 4 numerical simulation of transitional flow in a patient-specific intracranial aneurysm," J Biomech 44(16),
- 5 2826–2832 (2011).
- <sup>7</sup> Y. Utaka, S. Okuda, and Y. Tasaki, "Configuration of the micro-layer and characteristics of heat
- 7 transfer in a narrow gap mini/micro-channel boiling system," Int J Heat Mass Transf **52**(9–10), 2205–
- 8 2214 (2009).
- 9 8 X.L. Xie, W.Q. Tao, and Y.L. He, "Numerical Study of Turbulent Heat Transfer and Pressure Drop
- 10 Characteristics in a Water-Cooled Minichannel Heat Sink," J Electron Packag 129(3), 247–255 (2007).
- <sup>9</sup> Z. Cheng, T.O. Jelly, S.J. Illingworth, I. Marusic, and A.S.H. Ooi, "Forcing frequency effects on
- turbulence dynamics in pulsatile pipe flow," Int J Heat Fluid Flow 82, 108538 (2020).
- 13 <sup>10</sup> S. He, and J.D. Jackson, "An experimental study of pulsating turbulent flow in a pipe," European
- 14 Journal of Mechanics B/Fluids **28**(2), 309–320 (2009).
- 16 Fluids **13**(5), 1367–1384 (2001).
- 17 P.K. Papadopoulos, and A.P. Vouros, "Pulsating turbulent pipe flow in the current dominated
- regime at high and very-high frequencies," Int J Heat Fluid Flow **58**, 54–67 (2016).
- 19 13 D.M. Eckmann, and J.B. Grotberg, "Experiments on transition to turbulence in oscillatory pipe
- 20 flow," J Fluid Mech **222**(1), 329 (1991).
- 21 <sup>14</sup> M. Iguchi, G. Park, and Y. Koh, "The structure of turbulence in pulsatile pipe flows," KSME
- 22 Journal 7(3), 185–193 (1993).

- 1 15 R. Trip, D.J. Kuik, J. Westerweel, and C. Poelma, "An experimental study of transitional pulsatile
- pipe flow," Physics of Fluids **24**(1), 014103 (2012).
- 3 Leading 16 D. Xu, and M. Avila, "The effect of pulsation frequency on transition in pulsatile pipe flow," J
- 4 Fluid Mech **857**, 937–951 (2018).
- 5 To D. Xu, S. Warnecke, B. Song, X. Ma, and B. Hof, "Transition to turbulence in pulsating pipe flow,"
- 6 J Fluid Mech **831**, 418–432 (2017).
- 7 18 J.C. Stettler, and A.K.M.F. Hussain, "On transition of the pulsatile pipe flow," J Fluid Mech 170,
- 8 169–197 (1986).
- 9 19 M.C. Brindise, and P.P. Vlachos, "Pulsatile pipe flow transition: Flow waveform effects," Physics
- 10 of Fluids **30**(1), 015111 (2018).
- 11 <sup>20</sup> D. Morón, D. Feldmann, and M. Avila, "Effect of waveform on turbulence transition in pulsatile
- 12 pipe flow," J Fluid Mech **948**, A20 (2022).
- 13 <sup>21</sup> H.L. Falsetti, R.J. Carroll, R.D. Swope, and C.J. Chent, "Turbulent blood flow in the ascending,"
- 14 Cardiovasc Res 17, 427–436 (1983).
- 15 <sup>22</sup> T. Sarpkaya, "Experimental Determination of the Critical Reynolds Number for Pulsating
- Poiseuille Flow," Journal of Basic Engineering 88(3), 589–598 (1966).
- 17 23 F. Scarano, "Iterative image deformation methods in PIV," Meas Sci Technol 13(1), R1–R19
- 18 (2002).
- 19 24 A. Eckstein, and P.P. Vlachos, "Digital particle image velocimetry (DPIV) robust phase
- 20 correlation," Meas Sci Technol **20**(5), 055401 (2009).
- 21 25 A.C. Eckstein, J. Charonko, and P. Vlachos, "Phase correlation processing for DPIV
- 22 measurements," Exp Fluids **45**(3), 485–500 (2008).

- 1 26 A. Eckstein, and P.P. Vlachos, "Assessment of advanced windowing techniques for digital particle
- 2 image velocimetry (DPIV)," Meas Sci Technol **20**(7), 075402 (2009).
- 3 <sup>27</sup> J. Westerweel, and F. Scarano, "Universal outlier detection for PIV data," Exp Fluids **39**(6), 1096–
- 4 1100 (2005).
- 5 <sup>28</sup> L. Sirovich, "Chaotic dynamics of coherent structures," Physica D **37**(1–3), 126–145 (1989).
- 6 29 M.C. Brindise, and P.P. Vlachos, "Proper orthogonal decomposition truncation method for data
- denoising and order reduction," Exp Fluids **58**(4), 28 (2017).
- 8 30 J. ZHOU, R.J. ADRIAN, S. BALACHANDAR, and T.M. KENDALL, "Mechanisms for
- 9 generating coherent packets of hairpin vortices in channel flow," J Fluid Mech **387**, 353–396 (1999).
- 10 31 I.J. Wygnanski, and F.H. Champagne, "On transition in a pipe. Part 1. The origin of puffs and slugs
- and the flow in a turbulent slug," J Fluid Mech **59**(2), 281–335 (1973).